Thermal and Mechanical Energy Performance Analysis of Closed-loop Systems in Hot-Dry-Rock and Hot-Wet-Rock Reservoirs

Mark White[1], Mario Martinez[2], Yaroslav Vasyliv[2], Gabriela A. Bran-Anleu[2], Carlo Parisi[3], Paolo Balestra[3], Roland Horne[4], Chad Augstine[5], Laura Pauley[6], Doug Hollett[7], Giorgia Bettin[2], Theron Marshall[3], and the Closed Loop Geothermal Working Group[8]

[1]Pacific Northwest National Laboratory, Richland, Washington, USA

[2]Sandia National Laboratory, Albuquerque, New Mexico, USA

[3]Idaho National Laboratory, Idaho Falls, Idaho, USA

[4]Stanford University, Stanford, California, USA

[5]National Renewable Energy Laboratory, Golden, Colorado, USA

[6]Pennsylvania State University, University Park, Pennsylvania, USA

[7]Melroy-Hollett Technology Partners, Arlington, Virginia, USA

Keywords

Closed-loop geothermal systems, hot-dry-rock, hot-wet-rock, u-shaped borehole, coaxial borehole, numerical simulation, collaborative study

ABSTRACT

To understand the potential and limitations for recovering thermal and mechanical energy from closed-loop geothermal systems a collaborative study is underway that will investigate an array of system configurations, working fluids, geothermal reservoir characteristics, operational periods, and heat transfer enhancements. Closed-loop geothermal systems are distinguished from hydrothermal or enhanced geothermal systems (EGS) in that the working fluid only circulates through drilled boreholes. Principal objectives of this study are to determine upper limits for thermal and mechanical energy recovery and optimal operational and configuration parameters for each scenario. Teams of scientists and engineers are applying a suite of numerical simulation and analytical tools to model the heat recovery from closed-loop geothermal systems, and then

[8] D. Andrs, C. Augustine, S. Baek, P. Balestra, G. Bettin, D. Blankenship, L. Boyd, G. Bran Anleu, E. Brown, Z. Frone, D. Hollett, R.N. Horne, A. Kucala, C. Lam, J.B. Lechman, T.S. Lowry, T.D. Marshall, M. Martinez, L.L. Pauley, C. Parisi, S. Porse, C. Proctor, S.R. Subia, M.D. White, J. Winick, and Y.V. Yasyliv

optimizing operational and configuration parameters to maximize the thermal and mechanical energy recovery. Results from the suite of numerical simulators and analytical tools, such as outlet and inlet states and temperature profiles in the geothermal reservoir over time are intercompared to increase confidence in the analysis. This paper documents the study findings for closed-loop systems in hot-dry-rock reservoirs, where water is the working fluid. The characteristics of the hot-dry-rock reservoir were based on the U.S. Department of Energy's Utah Frontier Observatory for Research in Geothermal Energy (FORGE) site, near Milford Utah. Two objective functions are defined to optimize the operational and configuration parameters of the system, one each for the recovery of mechanical and thermal energy over the period of operation. For both objective functions, a surface plant thermal to mechanical energy conversion factor and an energy drilling cost is required. In keeping with the study objectives the surface plant conversion factor is determined from a second-law of thermodynamics analysis of a generic binary plant, and drilling costs are based on those from the Utah FORGE site and current national electrical costs.

1. Introduction

The Closed-Loop Geothermal Working Group project aims to determine upper limits for thermal and mechanical energy recovery for series of closed-loop geothermal system configurations, and host rock types (i.e., hot-dry-rock, hot-wet-rock), using multiple numerical simulation or analytical modeling approaches. For the purposes of this study, closed-loop geothermal systems refer to those geothermal systems where the working fluid does not directly contact the host rock. Investigations of closed-loop systems were initiated during an era where the focus was on hydrothermal and fractured hot-dry-rock systems (Kruger et al., 1981). Around this time, numerical and analytical models were developed to analyze closed-loop coaxial designs (Horne, 1980; Morita et al., 1985), and scoping field experiments were conducted with closed-loop coaxial designs with water as the working fluid (Kurasawa et al., 1981; Morita et al., 1985). Advances in directional drilling in high-temperature and high-pressure environments (Finger & Blankenship, 2010) has opened the possibilities for borehole configurations, including those that are u-shaped and multi-lateral u-shaped. The project will initially investigate water as the working fluid, starting with temperature and pressure conditions that keep water in a liquid state in the closed loop borehole, but will later consider alternative working fluids, including phase transitions, and novel system enhancements.

This paper reports on two closed-loop geothermal system configurations, a u-shaped borehole in a hot-dry-rock reservoir and a coaxial borehole in a hot-wet-rock reservoir. Comparisons of numerical simulation and analytical model results will be presented, along with the details of the numerical simulations executed with the Pacific Northwest National Laboratory's (PNNL's) STOMP-GT simulator with its embedded borehole and fracture capabilities (White et al., 2020). Details of simulations executed by Idaho National Laboratory (INL) with its coupled RELAP5 and 3D-PRONGHORN computer codes and Sandia National Laboratory (SNL) with its Sierra computer code (Team, 2021) will be reported in two companion papers, respectively (Parisi et al., 2021; Vasyliv et al., 2021). The reservoir characteristics for the hot-dry-rock scenario was based on the native state of the Utah Forge Site (Podgorney et al., 2020) and those for the hot-wet-rock scenarios were based on the HGP-A well on the island of Hawaii (Morita et al., 1992b).

2. U-Shaped Borehole in Hot-Dry-Rock Problem Description

Utah FORGE is an initiative, funded by the U.S. Department of Energy (DOE) for research and development of enhanced geothermal systems (EGS). The site is located on the southeast margin

of the Great Basin near the town of Milford, Utah, adjacent to the Roosevelt Hot Springs, and active hydrothermal resources. The characterization well 58-32 provided pore pressure, temperature, vertical stress, minimum horizontal stress, maximum horizontal stress versus elevation over the interval from -600 m to 1250 m. Temperatures at the lowest depth were about 200˚C and followed a nonlinear gradient (Podgorney et al., 2020). Thermal, geomechanical, and fracture properties for the granitoid reservoir were determined from field and laboratory measurements and modeling calibrations (Podgorney et al., 2020). The relevant hot-dry-rock reservoir properties, based on the Utah FORGE site, for the u-shaped borehole problem are shown in Table 1.

Table 1. Hot-dry-rock reservoir properties and thermal gradient.

Property	Units	Value
Bulk Thermal Conductivity	W/m K	3.05
Porosity		0.01
Bulk Specific Heat	J/kg K	790
Bulk Density	kg/m^3	2750
Geothermal Gradient (increasing ˚C with depth)	˚C/m	0.0788
Surface Temperature	˚C	25.0
Rock Intrinsic Permeability	m^2	10^{-18}

The borehole is steel cased with an outer diameter of 21.91 cm and wall thickness of 1.14 cm, with a trajectory that's vertical from the ground surface to a depth of 2189.73 m, then deviates at a rate of 5˚/100 ft (0.164˚/m) until horizontal (depth of 2539.01 m), extends horizontally, then deviates at a rate of 5˚/100 ft (0.164˚/m) until vertical, then returns to the ground surface. A schematic of the u-shaped borehole trajectory with a 10,000-m horizontal extent embedded in a computational domain is shown in Figure 1. The working fluid is liquid water and the heat transfer between the inner surface of the pipe casing follows the correlation of Gnielinski for turbulent flow (Gnielinski, 1975; Incropera & DeWitt, 2007), which is valid for the range of Prandtl and Reynolds numbers from $0.5 \leq Pr \leq 2{,}000$ and $3{,}000 \leq Re_D \leq 5{,}000{,}000$. The outlet pressure is held to maintain liquid water conditions. The system is to be optimized for cumulative thermal and mechanical energy via three independent parameters: 1) horizontal extent (i.e., spacing between vertical legs of the boreholes, 2) flow rate, and 3) insulation length on the ascending vertical leg. Heat loss through the insulated section was assumed to be negligible. The inlet temperature was fixed at 30˚C.

3. Coaxial Borehole in Hot-Wet-Rock Problem Description

Foundational experiments (Morita et al., 1992b) of a downhole coaxial heat exchanger were conducted in the upper 879.6 m length of the HGP-A well on the island of Hawaii, just south of Puu Honuaula. This University of Hawaii (UH) drilled geothermal well produced 12.6 kg/s with nearly equal amounts of liquid and steam at a surface temperature of 186˚C, and operated a 2.8 MW electric plant from 1981 to 1989. Lava from the Kilauea 2018 eruption buried the site. Three

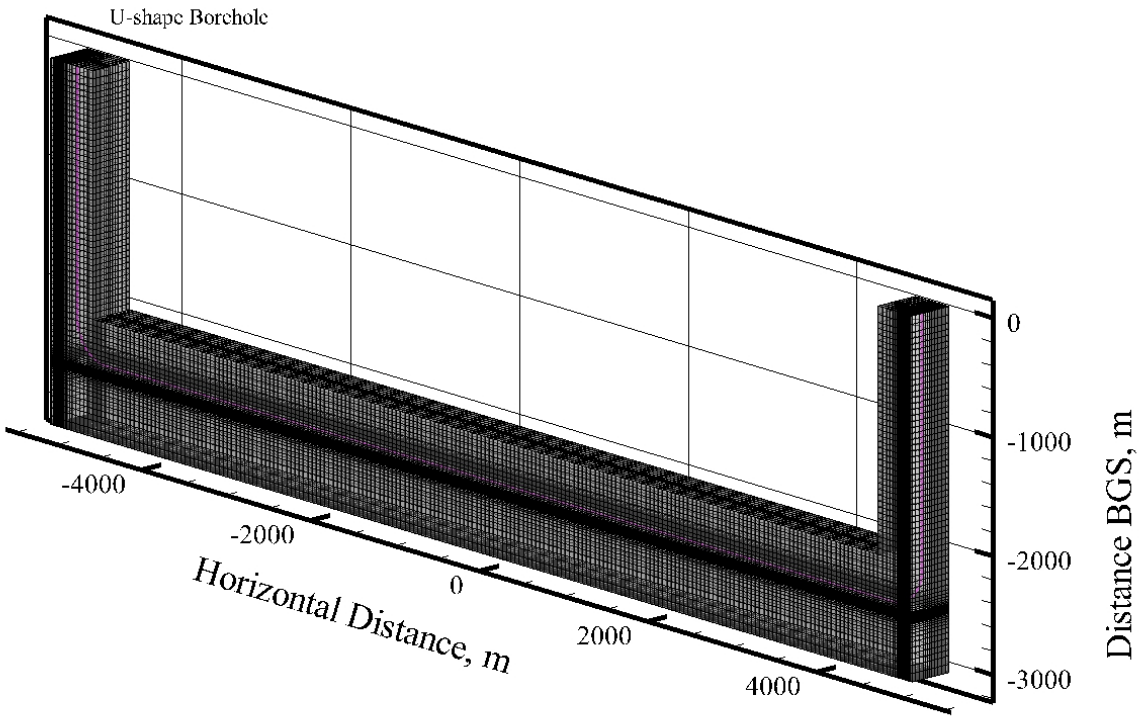

Figure 1: Well configurations for u-shaped borehole embedded in a computational domain.

problem scenarios were developed for this site for a coaxial closed-loop system configuration: 1) validation study of the experiment, 2) extension of the coaxial system to the bottom of the HGP-A well, and 3) extension of the coaxial system vertically and horizontally. The porosity and intrinsic permeability of the host rock at the Puu Honuaula site allowed for water circulation in contrast to the nearly impermeable rock of the Utah FORGE site, which distinguishes hot-wet-rock from hot-dry-rock. The relevant hot-wet-rock reservoir properties, based on the Puu Honuaula site, for the coaxial scenarios are shown in Table 2.

Table 2. Hot-wet-rock reservoir properties and thermal gradient.

Property	**Units**	**Value**
Grain Thermal Conductivity	W/m K	3.02
Porosity		0.133
Grain Specific Heat	J/kg K	965.0
Grain Density	kg/m^3	3,000
Geothermal Gradient (increasing ˚C with depth)	˚C/m	0.112
Surface Temperature	˚C	15.0
Rock Intrinsic Permeability	m^2	10^{-12}

The well configuration for the validation study (Scenario 1) was identical to that for the experiment (Morita et al., 1992b), as shown on the left-hand side in Figure 2. Cement fills the space between

the upper cased sections of the well. Properties of the well materials are shown in Table 3, where the insulated inner pipe was constructed as specified by Morita et al. (1988). The extended coaxial system configuration (Scenario 2) used a modified version of the actual experiment, sizes of the coaxial pipes being increased, but with area ratios between the inner pipe and outer annular space maintained to those of the experiment (i.e., 0.108), as shown on the left-hand side in Figure 2. This area ratio was designed to increase the residence time of the water in the outer annular space and minimize the residence time in the upward leg. The horizontal well configuration (Scenario 3) used the upper well configuration of Scenario 2, to a depth of 2189.73 m, then deviated at a rate of 5˚/100 ft (0.164˚/m) until horizontal (depth of 2539.01 m), then extended horizontally, as shown in Figure 3. The working fluid is liquid water and the heat transfer between water and pipe walls follows the correlation of Gnielinski for turbulent flow (Gnielinski, 1975; Incropera & DeWitt, 2007). Optimization of thermal and mechanical energy followed that of the hot-dry-rock problem.

Table 3. Well material properties.

Material	Density, kg/m^3	Specific Heat, J/kg K	Thermal Conductivity, W/m K
Casing Pipe (Steel)	7,850	470	46.1
Cement	1,830	880	0.93
Insulated Inner Pipe	3,925	235	0.07

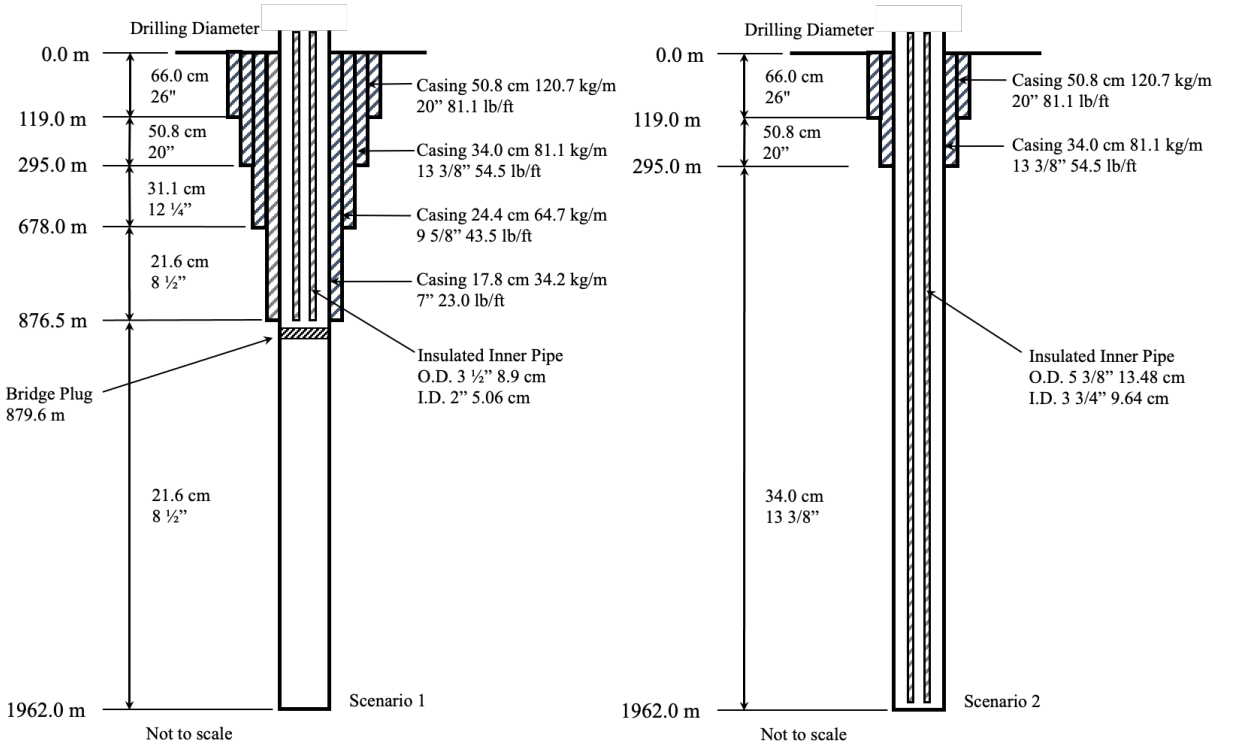

Figure 2: Well configurations for coaxial hot-wet-rock Scenarios 1 and 2.

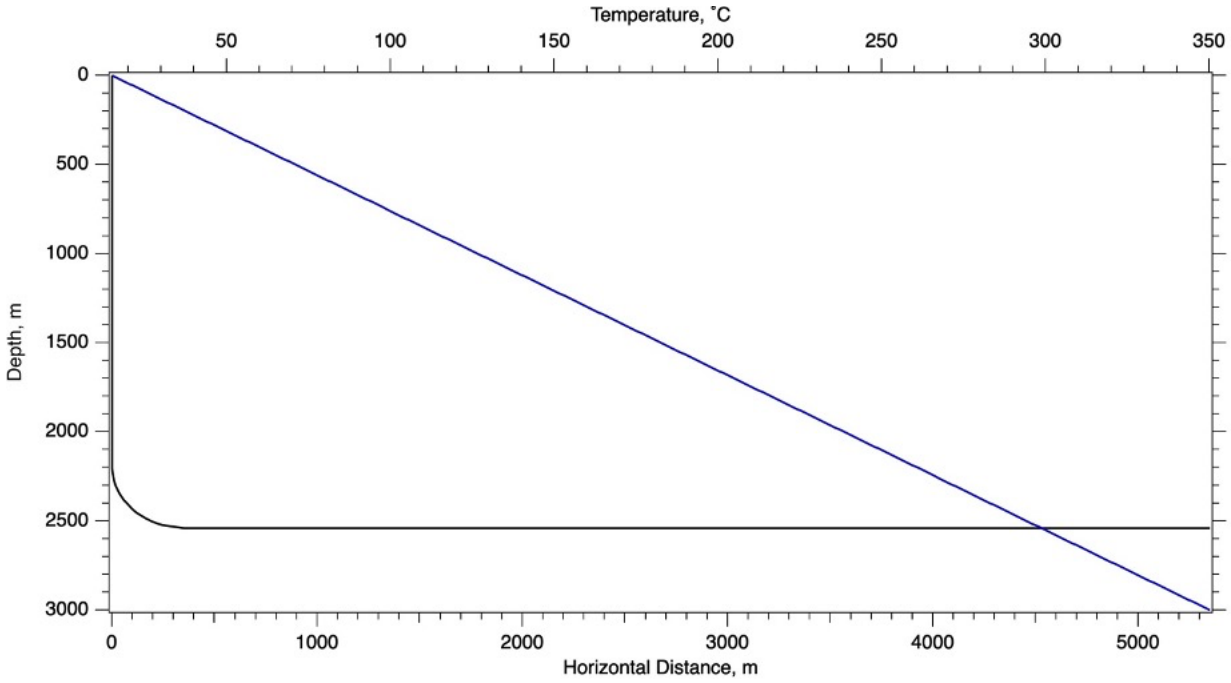

Figure 3: Well trajectory and temperature profile for coaxial hot-wet-rock Scenario 3.

4. Thermal and Mechanical Energy Objective Functions

A cumulative produced energy basis was selected to evaluate and optimize the performance of all of the closed-loop geothermal system configurations. Two objective functions were developed to optimize the cumulative produced thermal and mechanical energy. Conversion of mechanical to electrical energy is not considered. Both objective functions balance cumulative produced energy over the system lifetime, assuming continuous operation, with the energy cost of drilling, and pumping costs. Other capital and operating costs were not considered in this energy based analysis. To convert between produced thermal and mechanical power, a second-law based binary surface plant efficiency was developed. Produced thermal and mechanical energy are reported for a range of drilling costs. The net thermal power produced is the difference in enthalpy between the outlet and inlet water times the mass flow rate minus any pumping power required divided by the binary power efficiency and the pump efficiency:

$$\dot{m}\,[h_{out} - h_{in}] - \frac{\dot{m}}{\rho}\,\frac{\max\{[P_{in} - P_{out}],0\}}{\eta_b\,(T_{in},T_{out})\,\eta_p} \tag{1}$$

where h_{out} is the outlet enthalpy, J/kg; h_{in} is the inlet enthalpy, J/kg; $\dot{m}$ is the mass flow rate, kg/s; P_{in} is the inlet pressure, Pa; P_{out} is the outlet pressure, Pa; $\eta_b\,(T_{in}, T_{out})$ is the binary plant efficiency as a function of inlet and outlet temperature, η_p is the pump efficiency, and ρ is the average working fluid density. The net mechanical power is the mechanical work produced by the ideal binary plant minus any pumping power required:

$$\dot{m}\,W_b\,(T_{in}, T_{out}) - \frac{\dot{m}}{\rho}\,\frac{\max\{[P_{in} - P_{out}],0\}}{\eta_p} \tag{2}$$

where $W_b\ (T_{in}, T_{out})$ is the work produced by the binary power plant as a function of the inlet and outlet temperature. To determine the work produced by an ideal binary cycle power plant a second-law approach was taken, based on the schematic shown in Figure 4.

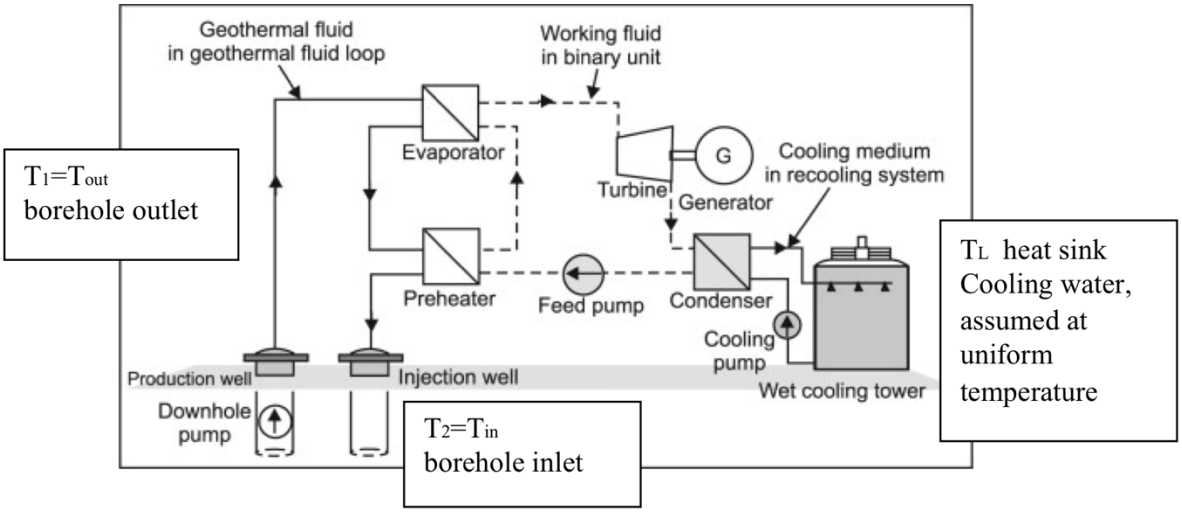

Figure 4: Surface binary power plant schematic.

Heat transferred into the binary cycle is the difference in outlet and inlet enthalpy times the mass flow rate:

$$\dot{Q}_H = \dot{m}\,[h_{out} - h_{in}] \tag{3}$$

where $\dot{Q}_H$ is the heat transferred into the cycle. A statement of the second law of thermodynamics is that the change in the entropy of the world must positive:

$$\Delta\dot{S}_{world} = \Delta\dot{S}_H + \Delta\dot{S}_L + \Delta\dot{S}_{cycle} > 0 \tag{4}$$

where $\Delta\dot{S}_{world}$ is the change in entropy of the world, W/K; $\Delta\dot{S}_H$ is the change in entropy on heat-source (H) side of the cycle (i.e., $\dot{m}\,[s_{out} - s_{in}]$), W/K; $\Delta\dot{S}_L$ is change in entropy on the heat-sink (L) side of the cycle, W/K; and $\Delta\dot{S}_{cycle}$ is the entropy generated by the cycle, W/K. For maximum power generation by the cycle, $\Delta\dot{S}_{world} = 0$ and $\Delta\dot{S}_{cycle} = 0$:

$$\Delta\dot{S}_H + \Delta\dot{S}_L = 0 \tag{5}$$

This allows the determination of the heat rejection from Eqn. (5), assuming reversible heat transfer (i.e., small temperature difference between the working fluid and cooling water):

$$\Delta\dot{S}_L = {\dot{Q}_L}\Big/{T_L} = \dot{m}\,[s_{out} - s_{in}] \tag{6}$$

For a low-sink temperature equal to 10˚C below the inlet temperature, an expression for the net power output of the binary cycle is obtained, which is essentially a function of inlet and outlet temperatures for liquid water:

$$\dot{W}_{net} = \dot{m}\,[h_{out} - h_{in}] - \dot{m}\,T_L\,[s_{out} - s_{in}] \tag{7}$$

where $\dot{W}_{net}$ is net power output of the cycle, W; T_L is the low-sink temperature (e.g., wet cooling tower), K; s_{out} is the entropy of the outlet working fluid, J/kg K; and s_{in} is the entropy of the inlet working fluid, J/kg K. The efficiency of the binary plant is then:

$$\eta_b = \dot{W}_{net} \Big/ \dot{m}\,[h_{out} - h_{in}] \tag{8}$$

Net thermal energy over the lifetime of the closed-loop geothermal system is the integrated net thermal power produced minus the thermal energy cost of drilling:

$$\int_0^{PL} \left(\dot{m}\,[h_{out} - h_{in}] - \frac{\dot{m}}{\rho} \frac{\max\{[P_{in} - P_{out}],0\}}{\eta_b\,(T_{in},T_{out})\,\eta_p} \right) dt - \int_0^{PL} \frac{L_{drilling}\,C_{drilling}}{\eta_b\,(T_{in},T_{out})\,C_{electric}\,PL}\,dt \tag{9}$$

where PL is the plant lifetime, s; t is time, s; $L_{drilling}$ is the overall drilling length, m; $C_{drilling}$ is the drilling cost, $/m; and $C_{electric}$ is the cost of electricity $/J. Net mechanical energy over the lifetime of the closed-loop geothermal system is the integrated net mechanical power produced minus the mechanical energy cost of drilling:

$$\int_0^{PL} \left(\dot{m}\,W_b\,(T_{in},T_{out}) - \frac{\dot{m}}{\rho} \frac{\max\{[P_{in} - P_{out}],0\}}{\eta_p} \right) dt - \frac{L_{drilling}\,C_{drilling}}{C_{electric}} \tag{10}$$

This analysis neglects the irreversibilities due to heat transfer across a temperature difference from the high-temperature reservoir to the working fluid in the cycle and from the working fluid to the low-temperature reservoir.

5. U-Shaped Borehole in Hot-Dry-Rock Problem Solutions

The principal objective of the hot-dry-rock problem was to determine maximum net mechanical and thermal energy production for a 40-year system life, with the horizontal extent (limited to 10,000 m), flow rate, and length of insulation in the ascending vertical leg being the independent parameters. Net thermal and mechanical energy were determined from the objective functions shown in Eqn. (9) and (10), respectively, with the produced energy being discounted by pumping costs and drilling costs. Four drilling costs were considered $0/m, $500/m, $1000/m, and $1500/m, yielding a series of eight optimal solutions to be determined (i.e., two energies x four drilling costs). This analysis was completed by SNL with their Sierra flow and transport code and Dakota package for the optimizations, with details provided in their companion paper (Vasyliv et al., 2021). For drilling costs up to $1500/m, the optimization analysis did not identify a optimal horizontal extent within the 10 km limit for either the net mechanical or thermal energy. Results from the optimization analysis are summarized in Table 4, where the cost of electricity in Eqn (9) and (10) was set to represent a national average of 10.45 cents/KWh (2.903 x 10^{-8} $/J). Optima for net mechanical energy was rather insensitive to the drilling-cost penalty in terms of resulting mass flow rates and insulation lengths. However, optima for net thermal energy had decreasing flow rates and increasing insulation lengths with increasing drilling costs; both of which resulted in increased outlet temperatures.

Table 4. Summary of the optimization analysis for net mechanical and thermal energy produced for a system life of 40 years.

Optimized Mechanical Energy Objective Function						
Drilling Costs, $/m	Net Mean Power, MW^m	Net Mechanical Energy, GWh^m	Outlet Temp., ˚C	Mass Flow Rate, kg/s	Insulation Length, m	Horizontal Extent, m
0	0.880	308.7	128.2	11.8	1174	10,000
500	0.674	236.3	127.6	11.9	1111	10,000
1000	0.470	164.8	129.2	11.6	1406	10,000
1500	0.264	92.5	128.2	11.8	1289	10,000
Optimized Thermal Energy Objective Function						
Drilling Costs, $/m	Net Mean Power, MW^{th}	Net Thermal Energy, GWh^{th}	Outlet Temp., ˚C	Mass Flow Rate, kg/s	Insulation Length, m	Horizontal Extent, m
0	6.80	2383	70.1	38.0	875	10,000
500	4.72	1654	77.2	31.4	747	10,000
1000	3.01	1057	97.6	20.1	1005	10,000
1500	1.59	558	113.4	15.1	1080	10,000

The mechanical and thermal energy objective functions were designed to represent theoretical maximums for recovered energy, discounting only for pumping and horizontal extent, and not considering other capital or operating costs. Even with horizontal extents of 10,000 m and an overall borehole length of 14,742 m, thermosiphon greatly reduced or negated the pumping energy, leaving the initial drilling cost as the principal penalty term in the objective functions. SNL simulation results for outlet temperature versus time are shown in Figure 5, for the eight optima. Outlet temperatures are dependent on flow rate, and the insulation lengths were generally correlated with the point at which the ascending borehole water temperature exceeded that of the formation. SNL simulation results for net mechanical and thermal energy versus time are shown in Figure 6, for the eight optima. After 40 years of system operation, the optimal solutions for net thermal energy varied between 6.0 and 7.8 times that of the net mechanical energy for the same drilling cost, which is reflective of the efficiency of the second-law based binary plant in converting thermal to mechanical energy. For actual systems binary plant efficiencies would be expected to be lower. Validation of the simulation results against field experiments was not possible, but verification of the results were completed via intercomparison of simulation and semi-analytical results. Comparisons of outlet temperatures for two of the optimal scenarios are shown in Figure 7, from simulations with SNL's Sierra code, PNNL's STOMP-GT code, and the Stanford semi-analytical solution (Horne & Shinohara, 1979). In spite of the differences in modeling approaches and underlying assumptions, the two simulators and semi-analytical solution showed excellent agreement in outlet temperatures over the course of the 40-year period.

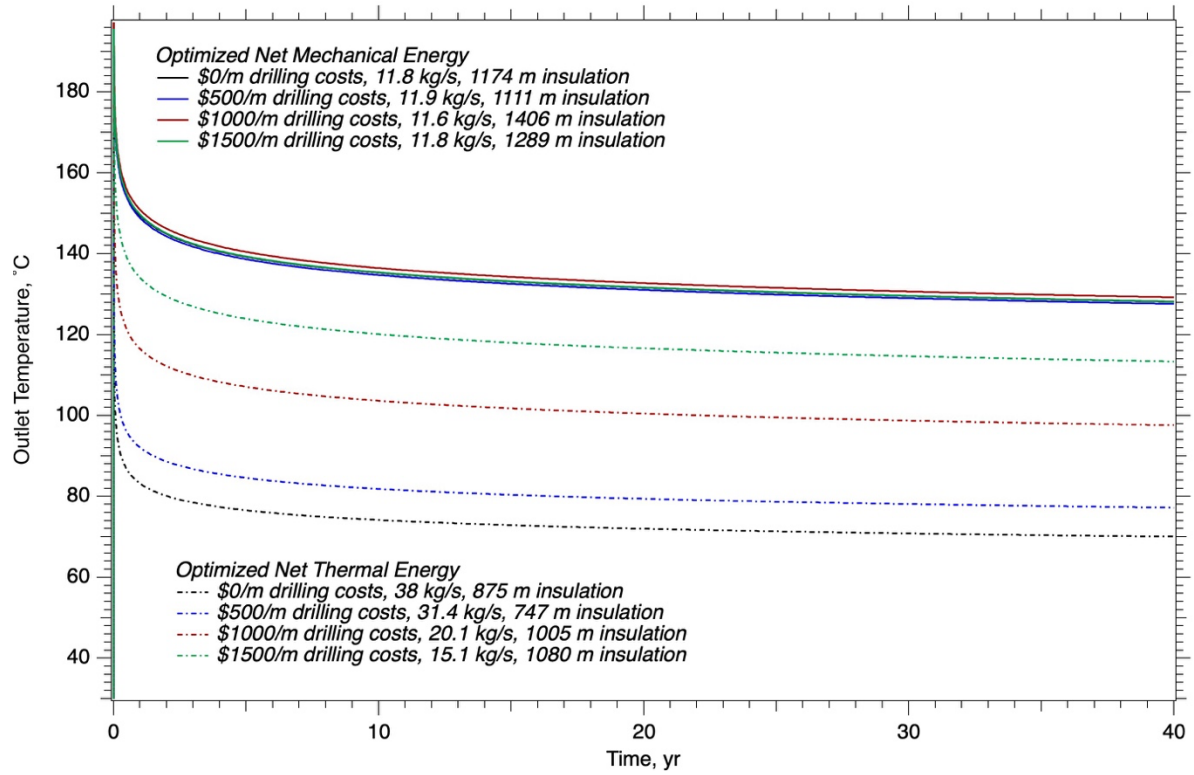

Figure 5: Outlet temperature versus time for optima solutions for net mechanical and thermal energy.

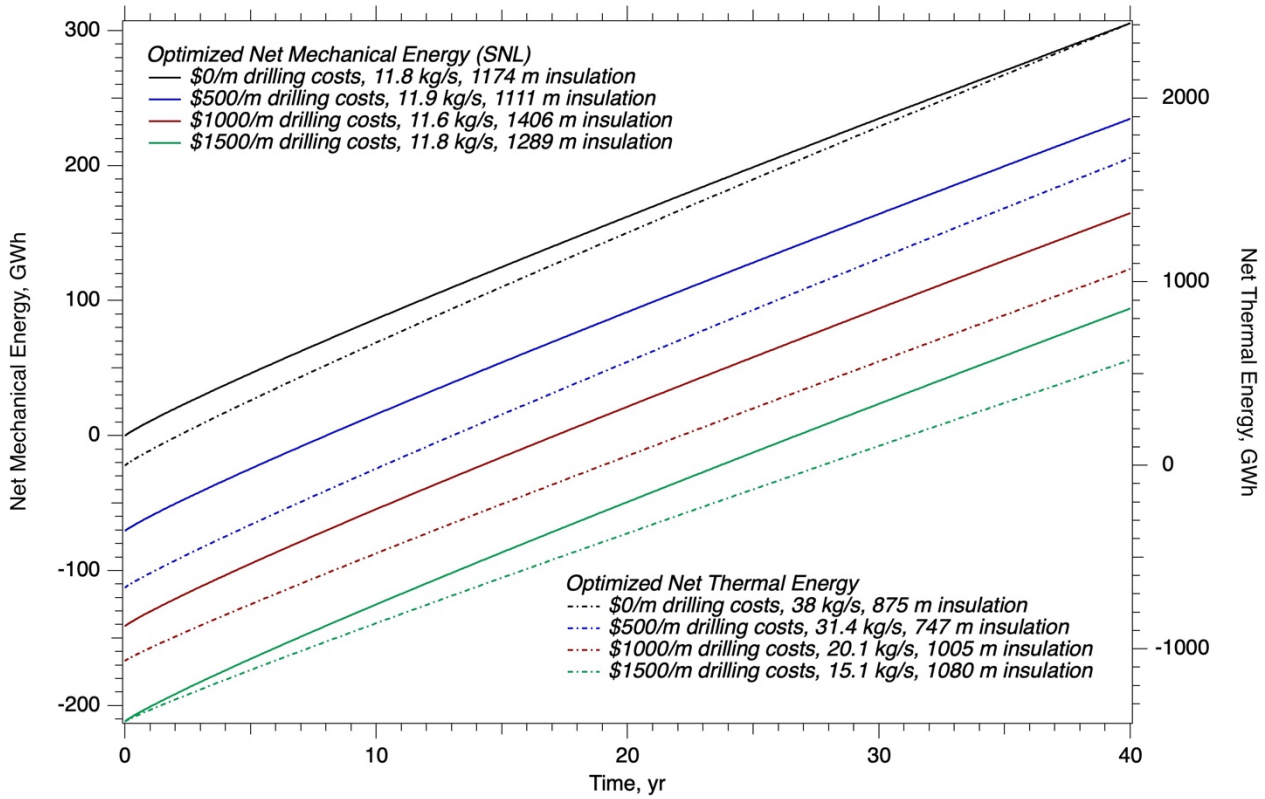

Figure 6: Net mechanical and thermal energy versus time for optima solutions for net mechanical and thermal energy.

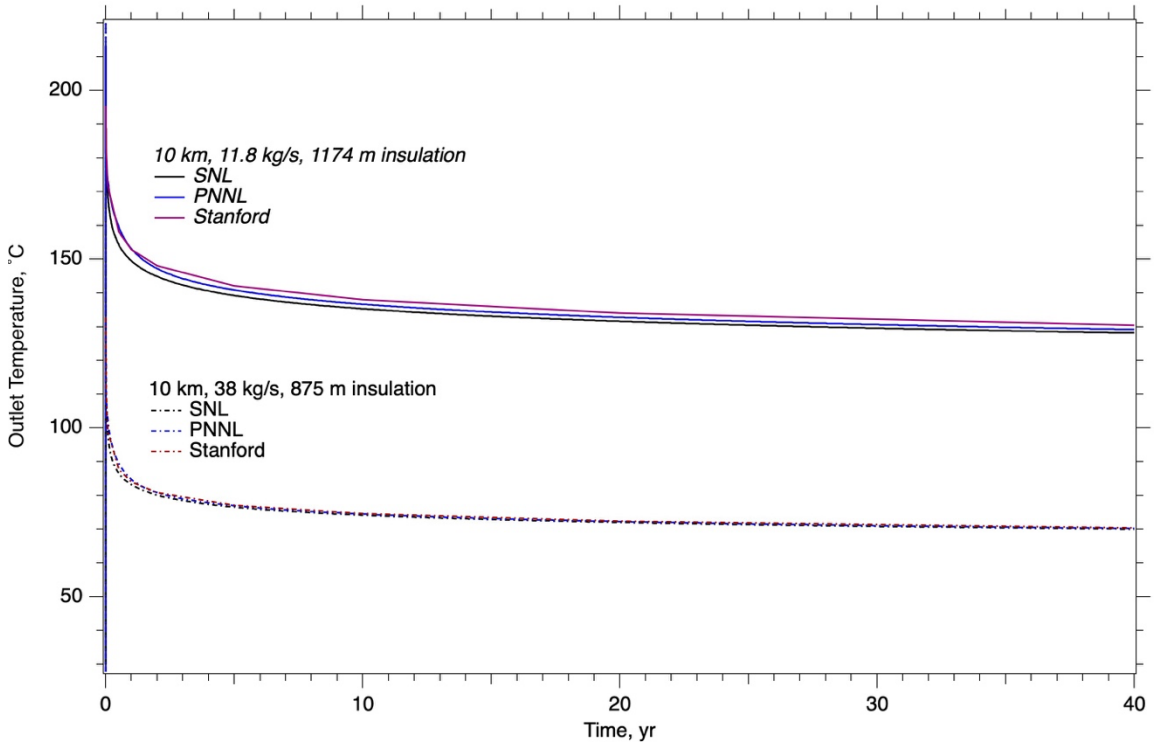

Figure 7: Comparison of outlet temperature versus time across numerical simulations and analytical solutions for optimal solutions at zero drilling costs.

6. Coaxial Borehole in Hot-Wet-Rock Problem Solutions

Numerical simulation and analytical solutions were generated against two scenarios of the coaxial hot-wet-rock problem. Solutions against the third problem scenario will be completed as part of the ongoing Closed Loop Geothermal Working Group project.

6.1 Scenario 1: Validation against the Downhole Coaxial Heat Exchanger Experiment

A critical outcome of the DCHE experiment (Morita et al., 1992b) was quantifying the thermal performance of the inner pipe. For this determination numerical simulations were executed that made the following assumptions: 1) heat is transferred to the wellbore from the rock only in the radial direction via conduction, and 2) the thermal capacitance of the inner pipe was negligible (Morita et al., 1992a). Experimental results in terms of produced water temperature were used to determine the effective formation and inner pipe thermal conductivity. Excellent agreement was found between the simulation and experimental results with effective thermal conductivities of the formation and inner pipe of 1.60 W/m K and 0.06 W/m K, respectively.

SNL and PNNL executed simulations against this scenario. The SNL approach followed that of Morita, ignoring the casing and cement and thermal capacitance of the inner pipe. The model geometry was a composite of two-dimensional axisymmetric or one-dimensional elements, as shown in Figure 8. PNNL modeled the experiment with coaxial borehole model embedded in porous media structured grid. Heat transfer between the basalt rock and coaxial borehole model was via a piece-wise Peaceman model with thermal conductivity replacing intrinsic permeability. For this model similar results were found with or without considering porosity and permeability.

The SNL simulation shows excellent agreement with the experimental measurements both during the early stages of the experiment (i.e., < 5.0 hours), later stages, as shown in Figure 9. To achieve good early stage agreement, it was necessary to use the measured experimental temperature profile shown in the inset to initialize the temperature of the basalt rock and borehole water. The PNNL simulation shows good general agreement with the experimental results, but with a sharper drop in outlet temperature during the transition period. Late time simulation results were most sensitive to the basalt rock thermal conductivity and insensitive to the permeability of the basalt rock.

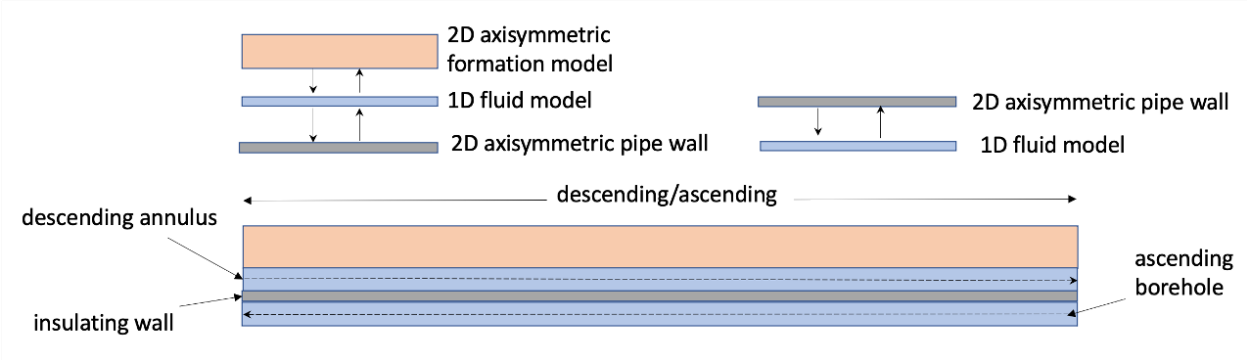

Figure 8: SNL downhole coaxial heat exchanger model.

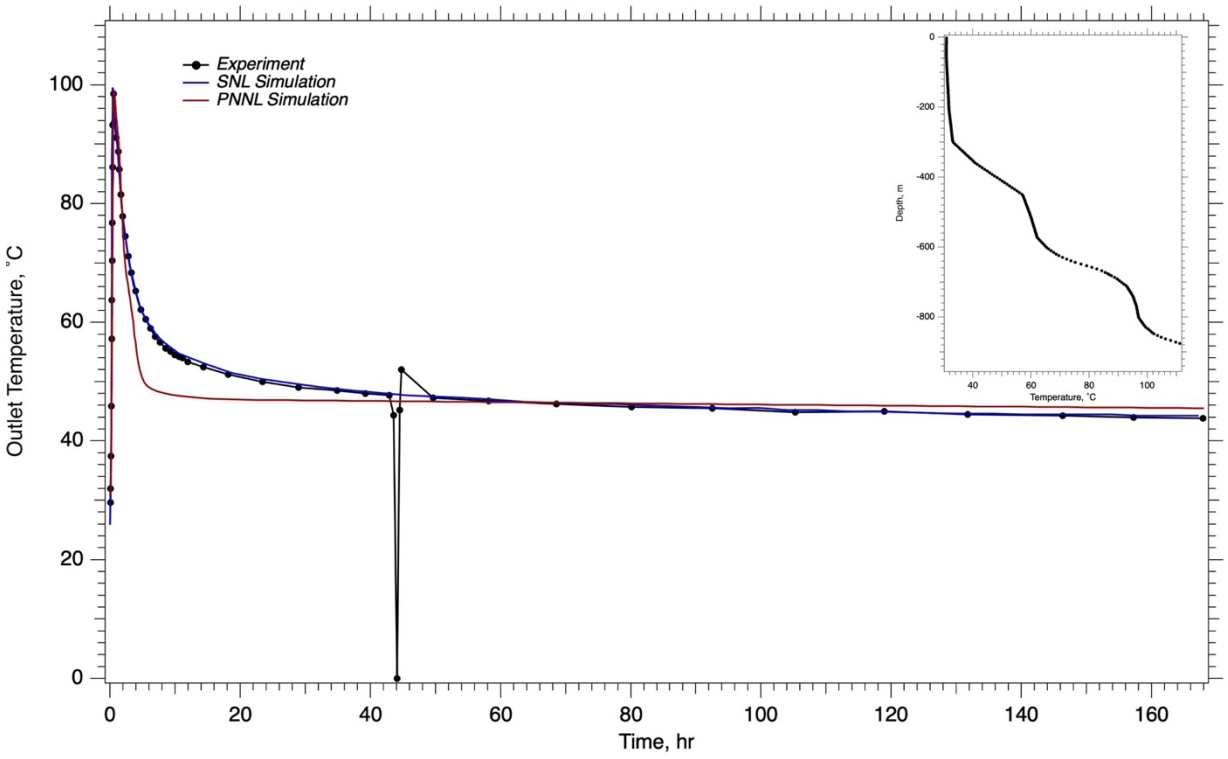

Figure 8: Comparisons of outlet temperature versus time between simulations and experiment for the hot-wet-rock Scenario 1 with experimental temperature profile inset.

6.2 Scenario 2: Vertical Extension of the Downhole Coaxial Heat Exchanger Experiment

Scenario 2 was designed to investigate a simple vertical extension of the DCHE experiment (Morita et al., 1992b) to the total original depth of the HGP-A well at 1962 m, below ground surface. For this scenario, a linear temperature gradient was assumed, and the initial temperature of the basalt formation and borehole water were set to this gradient. Formation water was allowed to circulate under natural convection forces, driven by density differences that occurred with changes in temperature of the formation water. The well completion was simplified and the dimensions of the coaxial system were increased. PNNL considered three flow rates: 5, 10, and 20 kg/s and two inlet temperatures: 30˚ and 60˚C. SNL considered two flow rates: 1.33 and 5 kg/s, an inlet temperature of 30˚C, and basalt permeabilities of 0.0 and 1.0 Darcy. PNNL simulation results for the 60˚ inlet temperature conditions are shown in Figure 10, in terms of temperature and binary plant efficiency versus time, and Figure 11, in terms of thermal and mechanical power and energy versus time. The results demonstrate the balance between flow rate and outlet temperature, with higher flow rates yielding lower outlet temperatures, as the residence time for fluid contact with the outer pipe wall decreases. Interestingly though the net impact on both thermal and mechanical power and energy is minimal, with slight improvements with faster flow rates for thermal power and energy and with slower rates for mechanical power and energy. For all cases, outlet temperatures are low and natural convection in the formation is counterproductive with downward flow yielding cooling. Energy flow into the coaxial system is largely controlled by the conduction between the outer pipe wall and formation. Energy loss between the inner and outer flows is nearly negligible with an effective thermal conductivity of 0.07 W/m K.

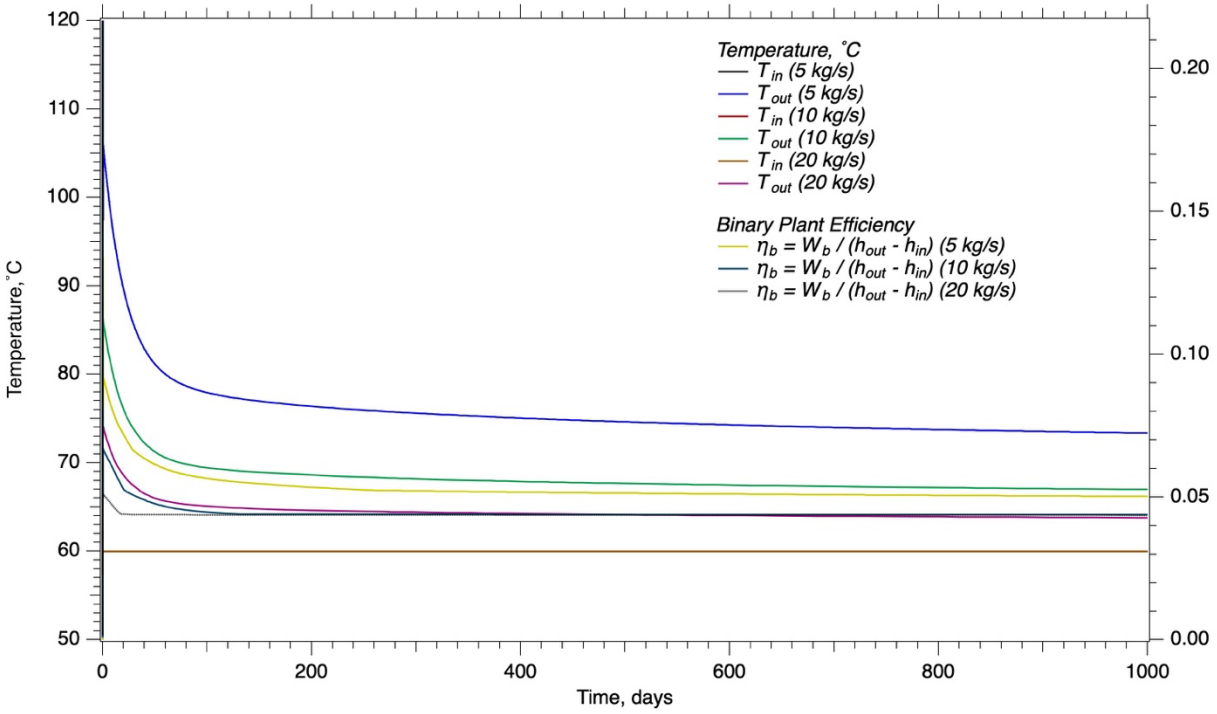

Figure 10: Outlet temperature and binary plant efficiency versus time for Scenario 2, 60˚C inlet.

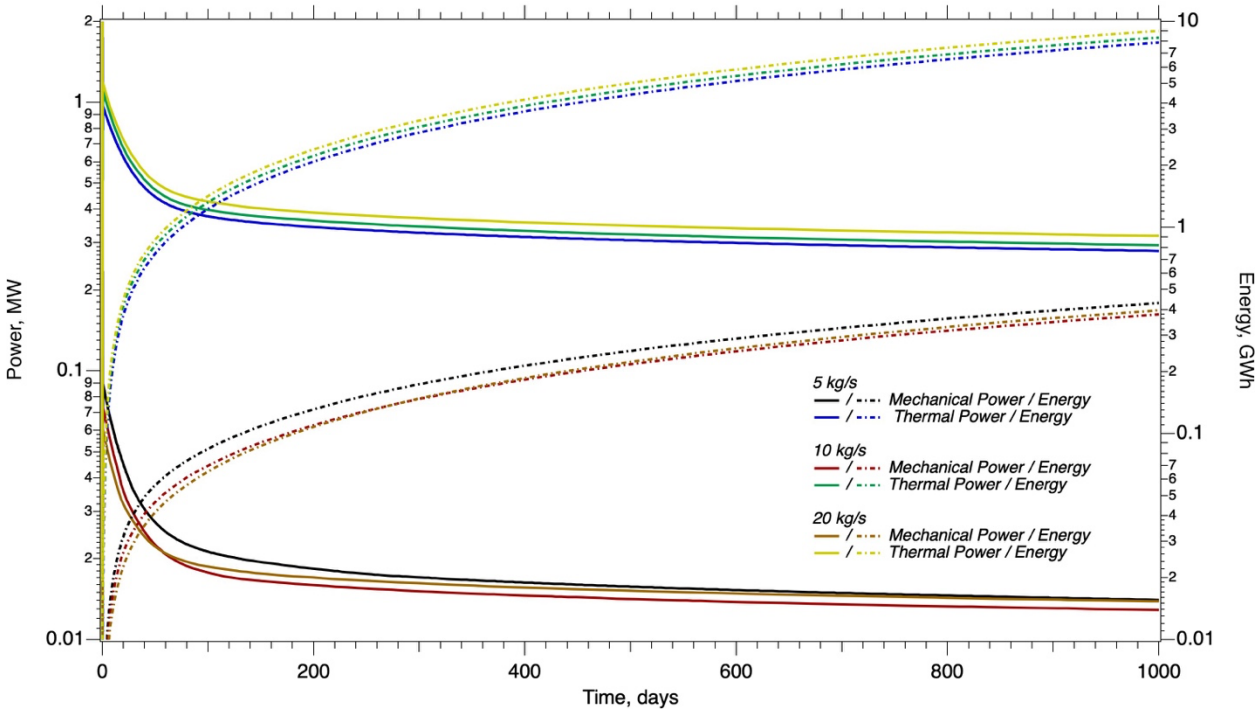

Figure 11: Thermal and mechanical power and energy versus time for Scenario 2, 60˚C inlet.

SNL and PNNL simulation results for the 30˚C inlet temperature conditions are shown in Figure 12 for temperature and binary efficiency versus time, and in Figure 13 for thermal and mechanical power versus time. Comparing the PNNL results for thermal and mechanical power

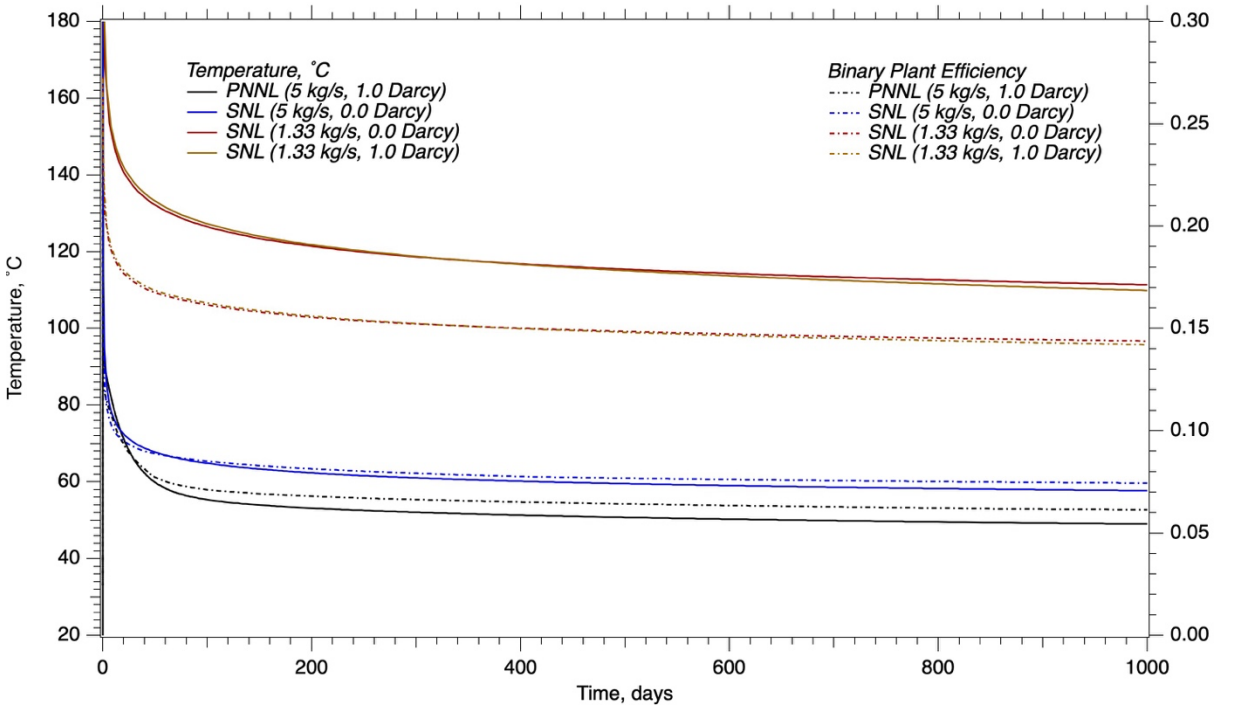

Figure 12: Outlet temperature and binary plant efficiency versus time for Scenario 2, 30˚C inlet.

against those for an inlet temperature of 30˚C, in Figure 8, shows that power generation is relatively insensitive to inlet temperature, with a slight advantage to a lower inlet temperature. Both thermal and mechanical power produced is also relatively insensitive to the flow rate, across all of the simulations from 1.33 to 20 kgs. This outcome is evidence that the system is controlled by the rate of heat conduction from the formation to the outer pipe. SNL investigated the impact of water circulation in the formation by considering two formation permeabilities, 0.0 and 1.0 Darcy, where the 0.0 Darcy case was equivalent to pure conduction. Simulation results shown in Figures 12 and 13, show that water circulation is detrimental to system performance, as natural convection circulation loop forms, with water flowing downward near the coaxial outer pipe, and upward radially farther from the center. This effectively brings cooler water in contact with the formation at lower depths, reduces the temperature slightly in that region. The impact to outlet temperature and produced thermal and mechanical energy is small. Results from all of the extended coaxial simulations in terms of average power production are summarized in Table 5.

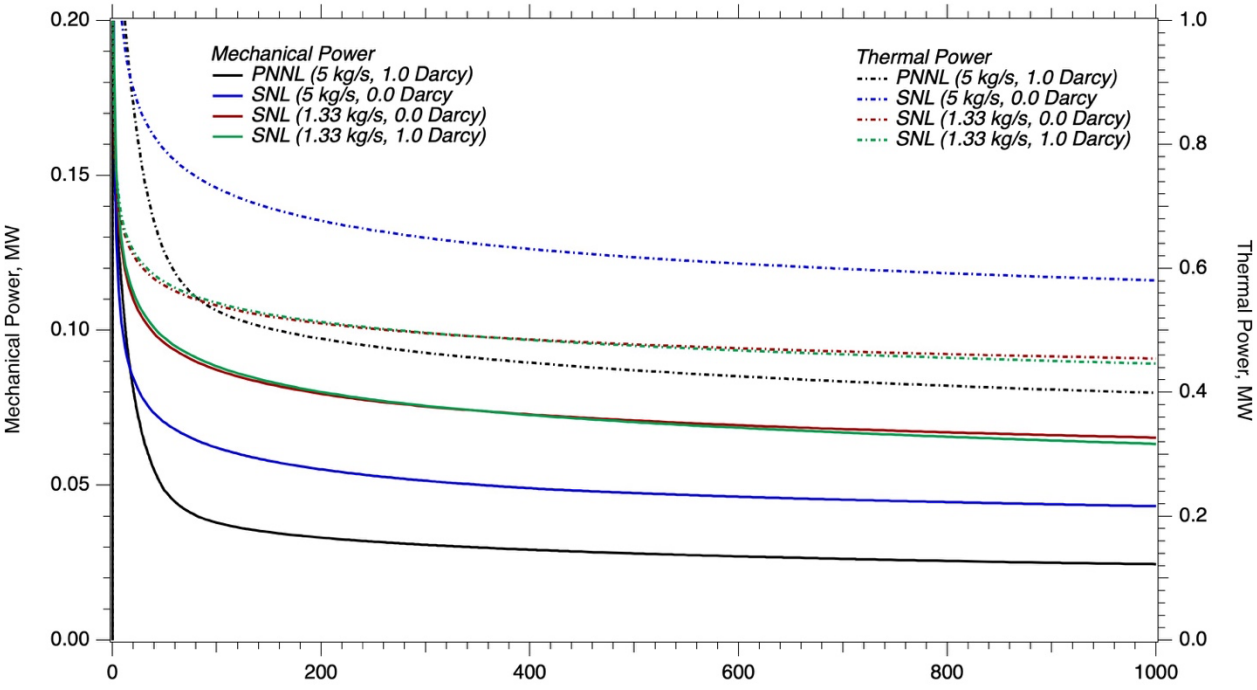

Figure 13: Thermal and mechanical power versus time for Scenario 2, 30˚C inlet.

Table 5. Summary of average power production for the Scenario 2 simulations .

Mass Flow Rate, kg/s	Permeability, Darcy	Inlet Temp., ˚C	Average Mechanical Power, MW^m	Average Thermal Power, MW^{th}
1.33	1.0	30.0	0.0513	0.390
5.0	1.0	30.0	0.0318	0.467
5.0	1.0	60.0	0.0184	0.339
10.0	1.0	60.0	0.0571	1.29
20.0	1.0	60.0	0.0751	1.72

7. Conclusions

Closed-loop geothermal systems avoid the complexities of establishing and maintaining hydraulic circulation in hot-dry-rock environments and producing formation water from hot-wet-rock environments by eliminating the direct contact of the working fluid with the formation rock. The closed-loop geothermal system approach, however, eliminates the created large fluid-rock contact surface area of enhanced geothermal systems in hot-dry-rock environments, achieved through hydraulic or shear-slip fracturing, or the inherent large fluid-rock surface area in hot-wet-rock environments via diffusive flow through porous media or highly fractured rock. The challenge then for closed-loop geothermal systems is to realize economically viable thermal or mechanical energy production via borehole configurations, working fluids, and external enhancements. To understand the potential and limitations of closed-loop geothermal systems for recovering thermal and mechanical energy a collaborative study is currently underway that will investigate an array of system configurations, working fluids, geothermal reservoir characteristics, operational periods, and heat transfer enhancements. This paper reports on results of this study for two environments (i.e., hot-dry-rock and hot-wet-rock) and two classical borehole configurations (i.e., u-shaped and coaxial heat exchanger), with liquid water as the working fluid. Future directions for the study include consideration of more modern borehole configurations, alternative working fluids (e.g., two-phase, thermo-catalytic, nonaqueous), and external, near-borehole enhancements (e.g., conductive-material-filled fractures, naturally circulating fractures).

An energy basis was chosen for assessing system performance of two closed-loop geothermal systems: 1) u-shaped borehole in an unfractured hot-dry-rock environment, and 2) a coaxial downhole heat exchanger in a permeable hot-wet-rock environment. Nominal borehole diameters were selected for both systems. An objective function was developed to optimize system performance that balanced produced thermal or mechanical energy against pumping and drilling costs. Pumping costs, in terms of mechanical energy, were determined from the inlet-outlet pressure differential, flow rate, fluid density, and pump efficiency. Drilling costs, in terms of mechanical energy, were determined from borehole length, electricity rates, and per-length drilling costs. Four per-length drilling costs were considered: \$0/m, \$500/m, \$1000/m, and \$1500/m. Mechanical energy produced or needed for pumping was created through a second-law based binary surface plant from produced thermal energy. The second-law based binary surface plant yielded efficiencies slightly below the thermodynamic limit of Carnot efficiency. For the two systems investigated thermo-siphon effects kept pumping costs to near negligible levels. For the closed-loop system in hot-dry rock, no optimal solution was determined below the horizontal extent length of 10,000 m. Optimal solutions were determined for mechanical and thermal energy produced over a 40-year period, assuming continuous operation for flow rate and insulation length. Optima for flow rate and insulation length showed greater dependence on drilling costs for mechanical than thermal energy.

For both closed-loop borehole configurations and environments, heat transfer between the formation rock and working fluid is dominated by thermal conduction from the rock to the borehole casing. Resistance to heat flow across the borehole casing and from the inner casing wall to the working fluid is nearly negligible. Optimal solutions for the insulation length of the ascending leg of the u-shaped borehole, were generally found at the transition point between fluid and formation rock temperature (i.e., the point at which the working fluid temperature becomes greater than the formation rock temperature). Working fluid temperature drop from the start of the ascending insulation leg in either the u-shaped or coaxial configurations were minimal, and an area

ratio of 10:1 between the outer and inner pipe of the coaxial configuration yielded a balance between resistance time for the descending and ascending fluid paths, without realizing excessive flow resistance. For the vertical coaxial borehole configuration, formation permeability resulted in a circulating flow pattern for the formation water, driven by fluid density differences, which slightly reduced performance over an impermeable formation, due to the downward flow transporting cooler water deeper in the formation.

Without discounting for drilling costs, the average power generation for the u-shaped borehole in the hot-dry-rock environment, with characteristics of the Utah FORGE site, for a horizontal extent of 10,000 m and an overall borehole length of 14,742 m, was 6.80 MW^{th} and 0.88 MW^{m}, using a second-law based binary plant efficiency. For the downhole coaxial heat exchanger borehole in the hot-wet-rock environment, with characteristics of the HGP-A well at the Puu Honuaula site with an overall vertical borehole extent of 1962 m, the average power generation was 1.72 MW^{th} and 0.075 MW^{m}.

Acknowledgements

This material was based upon work supported by the U.S. Department of Energy, Office of Energy Efficiency and Renewable Energy (EERE), Office of Technology Development, Geothermal Technologies Office, under Award Number DE-AC05-76RL01830 with PNNL and other awards to other national laboratories. The United States Government retains, and the publisher, by accepting the article for publication, acknowledges that the United States Government retains a non-exclusive, paid-up, irrevocable, world-wide license to publish or reproduce the published form of this manuscript, or allow others to do so, for United States Government purposes. This work is guided by an expert panel comprising Doug Hollett (Melroy-Hollett Technology Partners), Roland Horne (Stanford University), Laura Pauley (Pennsylvania State University), and Chad Augstine (National Renewable Energy Laboratory). We recognize and appreciate their dedication to the study and have greatly benefitted from their suggestions and reviews of the work.

REFERENCES

Finger, J., & Blankenship, D. (2010). *Handbook of Best Drilling Practices for Geothermal Drilling*. Retrieved from Sandia National Laboratory:

Gnielinski, V. (1975). Neue Gleichungen für den Wärme- und den Stoffübergang in turbulent durchströmten Rohren und Kanälen. *Forsch. Ing.-Wes., 41*(1), 8-16.

Horne, R. N. (1980). Design considerations of a down-hole coaxial geothermal heat exchanger. *Geothermal Resources Council Transactions, 4*, 569-572.

Horne, R. N., & Shinohara, K. (1979). Wellbore Heat Loss in Production and Injection Wells. *Journal of Petroleum Technology, 31*(1), 116-118. <Go to ISI>://WOS:A1979GG67400074

Incropera, F. P., & DeWitt, D. P. (2007). *Fundamentals of Heat and Mass Transfer* (6th ed.): Hoboken: Wiley.

Kruger, P., Ramey, H. J., Miller, F. G., Horne, R. N., Brigham, W. E., Donaldson, I. G., & Gudmundsson, J. S. (1981). *Proceedings of the Seventh Workshop on Geothermal-Reservoir Engineering*. Retrieved from

Kurasawa, T., Natume, S., & Takahashi, M. (1981). Report of heat exchange in a hot dry well. *Journal of New Energy Foundation, 6*, 29-44.

Morita, K., Bollmeier, W. S., & Mizogami, H. (1992a). Analysis of the results from the downhole coaxial heat exchanger (DCHE) experiment in Hawaii. *Geothermal Resources Council Transactions, 16*, 17-23.

Morita, K., Bollmeier, W. S., & Mizogami, H. (1992b). An experiment to prove the concept of the downhole coaxial heat exchanger (DCHE) in Hawaii. *Geothermal Resources Council Transactions, 16*, 9-16.

Morita, K., Matsubayashi, O., & Kusunoki, K. (1985). Down-hole coaxial heat exchanger using insulated inner pipe for maximum heat extraction. *Geothermal Resources Council Transactions, 9*, 45-50.

Morita, K., Morimoto, M., & Mukai, R. (1988, 10-14 Nov 1988). *Development of highly insulated inner pipe for downhole coaxial heat exchanger.* Paper presented at the International symposium on geothermal energy, Kumamoto, Japan.

Parisi, C., Balestra, P., & Marshall, T. D. (2021). Geothermal Analysis modeling and simulation using Idaho National Laboratory' RELAP5-3D-PRONGHORN coupled codes. *Geothermal Resources Council Transactions, 45*.

Podgorney, R. K., Finnila, A., Ghassemi, A., McLennan, J., & Moore, J. (2020, February 10-12, 2020). *Reference Native State and Stimulation Models of the Utah FORGE Site.* Paper presented at the 45th Workshop on Geothermal Reservoir Engineering, Stanford University.

Team, S. T. F. D. (2021). *SIERRA Multimechanics Module: Aria User Manual - Version 5.0*. Retrieved from Albuquerque, NM:

Vasyliv, Y. V., Bran-Anleu, G. A., Kucala, A., Subia, S., & Martinez, M. J. (2021). Analysis and optimization of a closed loop geothermal system in hot dry rock reservoirs. *Geothermal Resources Council Transactions, 45*.

White, M. D., Fu, P., & Team, E. C. (2020, February 10-12, 2020). *Application of an Embedded Fracture and Borehole Modeling Approach to the Understanding of EGS Collab Experiment 1.* Paper presented at the 45th Workshop on Geothermal Reservoir Engineering, Stanford University, Stanford, California.